

scale. Figure 21 shows the Ni-Cr-Mo-Gd alloy after corrosion testing. The bright areas are due to the gadolinide phase particles, which appear to be partially removed. Figure 21C shows the area of an entire MCA tooth where the gadolinide under the tooth is removed while the surrounding material is still intact. Figure 21A and B shows the edge of the crevice former where the inner gadolinides are removed, while gadolinides outside the crevice appear intact.

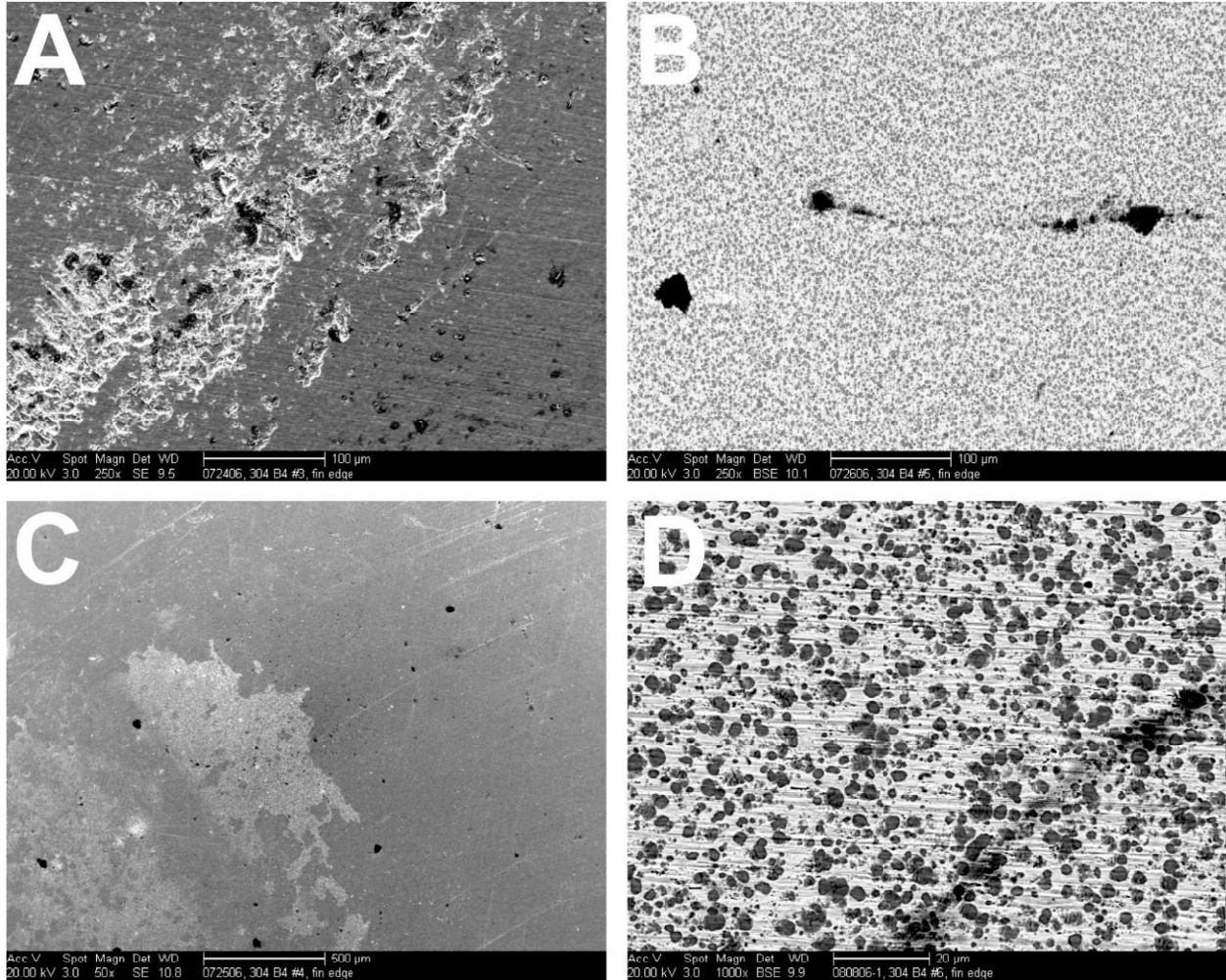


Figure 20. Scanning electron microscopy (SEM) images of 304B4 alloy corrosion specimens following testing. The images were obtained in SE (A and C) and backscatter electron (BSE) (B and D) modes.

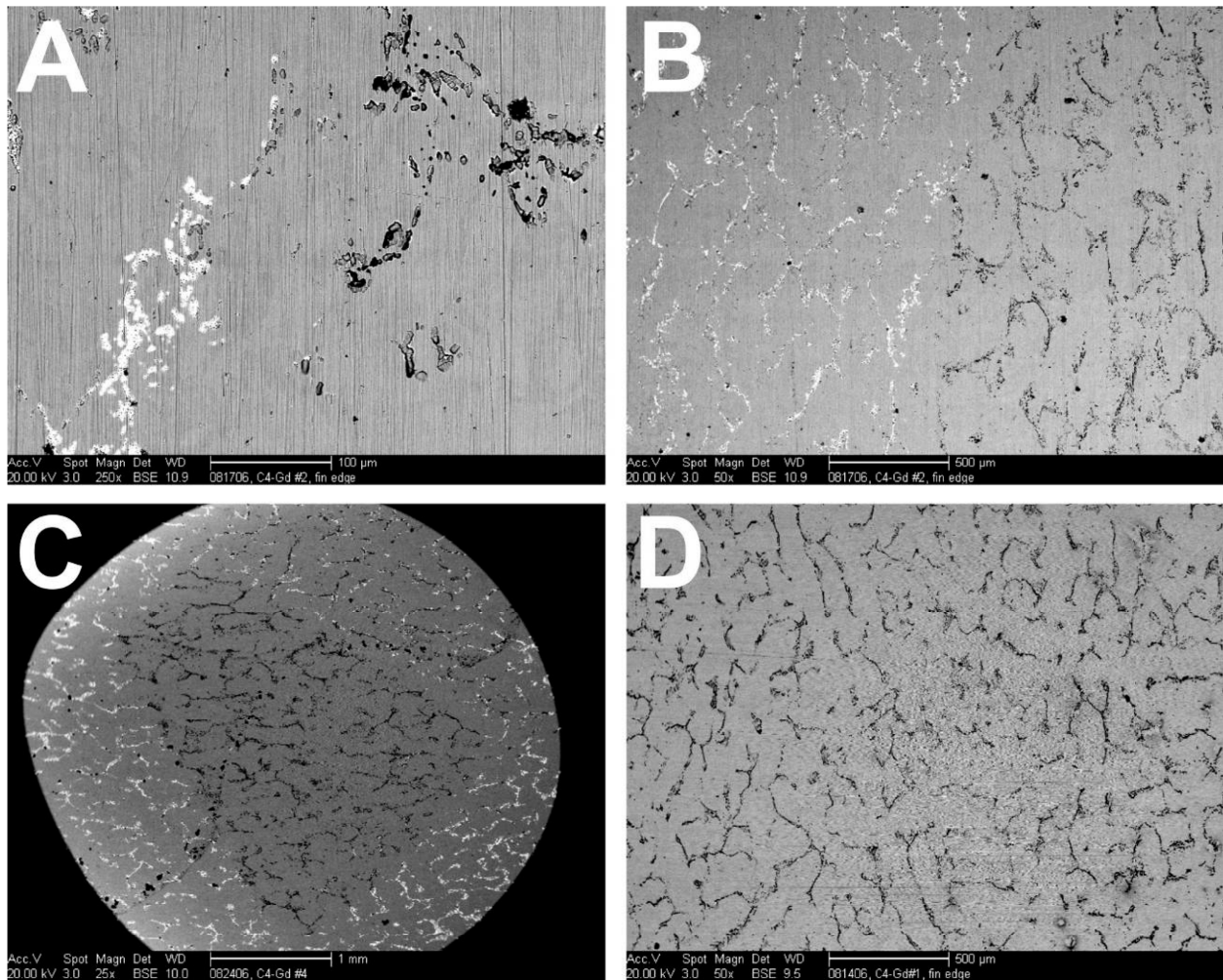


Figure 21. SEM images of Ni-Cr-Mo-Gd alloy corrosion specimens following testing. The images were obtained in BSE mode.

Additional SEM work was performed to show the microstructure of the secondary phases after testing. The SEM images were obtained in BSE mode to enhance the contrast of the secondary phase. Figure 22A and B shows the microstructure of the A978 alloy (Test 080206), with large secondary-phase particles compared with the 304B4 specimen (Test 080806-1), having smaller, more evenly distributed secondary-phase particles. The SEM image of the Ni-Cr-Mo-Gd specimen from Test 082406 shows the partial removal of the gadolinide phase. Small cavities remain from particles that were dissolved. No evidence of localized corrosion damage extending beyond these cavities was found.

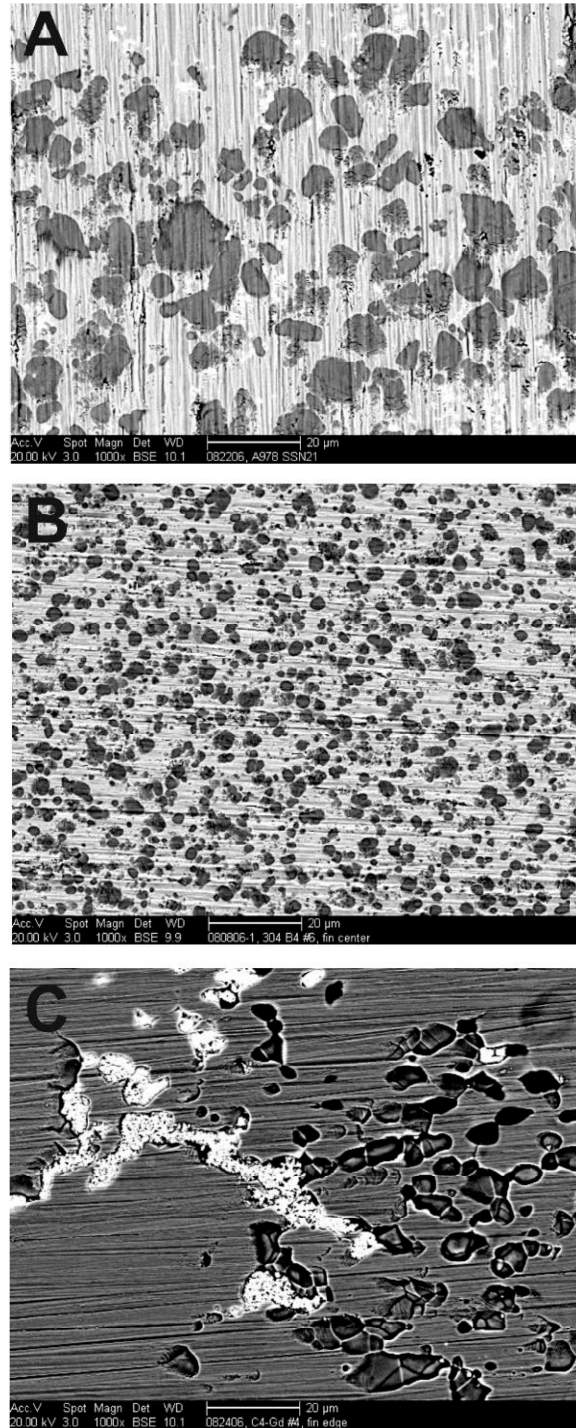


Figure 22. SEM images obtained in BSE mode showing the secondary phase particles for (A) A978, (B) 304B4, and (C) Ni-Cr-Mo-Gd alloys.

3.2.9 Post-test Analysis of Alloy 22 and Ni-Cr-Mo-Gd Test Specimens

Figure 23 shows photographs of the specimens after descaling. All the specimens show a similar amount of damage and number of crevice corrosion sites attacked. There was a difference in the amount

of crevice corrosion from one side to the other. This is likely due to the N₂ purge affecting the chemical transport, with the side most affected having less crevice attack. There are some differences in the attack of the Ni-Cr-Mo-Gd alloys versus Alloy 22. The Alloy 22 attack was more at the edges of the crevice tooth, while the Ni-Cr-Mo-Gd is more uniform across the crevice tooth. There is more pronounced staining of the Alloy 22 specimen.

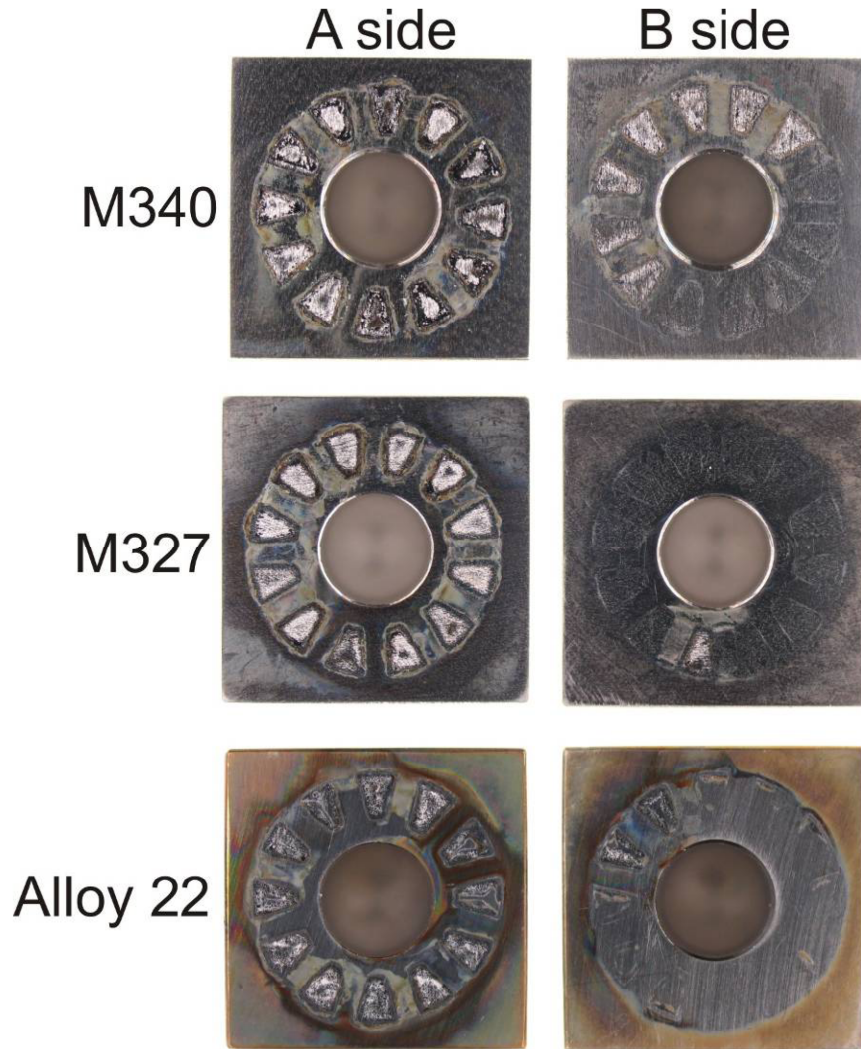


Figure 23. Macro photographs of the three alloys after descaling. The most damaged side is in the “A” column, and the less damaged side is in the “B” column.

3.2.10 Post-Test Analysis of Borated Stainless Steel Using an Optical Profilometer

Figure 24 shows optical profilometer data acquired on Neutrosorb Plus 304 stainless steels after corrosion testing. Figure 24A shows the extensive crevice corrosion damage to 304B6 at the Teflon compression gasket during exposure to solution B3 at 60°C at E_{corr} . Figures 24B and C show damage from a PS test for 304B4 under the Teflon MCA. Figure 24B shows what appears to be removal of material around secondary-phase particles in what could be the initiation of localized corrosion. Figure 24C shows the edge of a crevice corrosion pit where islands of material, on the same level as the polished surface, remain. These islands are likely secondary-phase particles (borides) that had not been released from the surface as the stainless steel austenite matrix was etched around them.

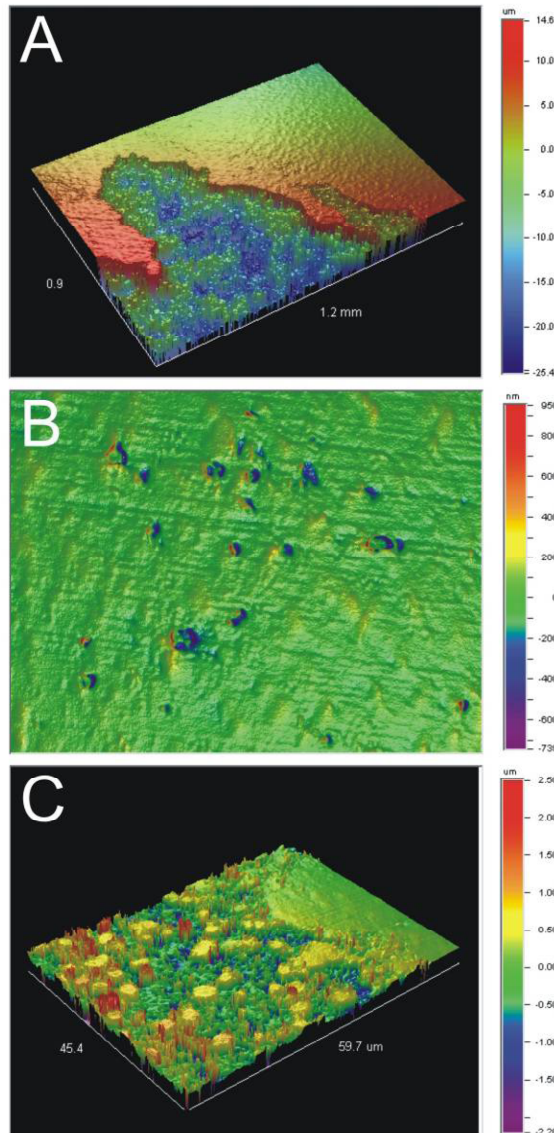


Figure 24. Optical profilometer data of specimens after corrosion experiments. (A) is 304B6 after E_{corr} measurement for 4 weeks in solution B3, and (B) and (C) are the 304B4 specimen damage from under the Teflon crevice former after the PS test at 0.1 V in solution B3.

4. CORROSION PRODUCT ANALYSIS

4.1.1 Corrosion Product Analysis of Grade A Borated Stainless Steels

Prior work has identified the composition of the borides found in Grade A material to be a Cr_2B type with a composition in weight percent of Cr-46, Fe-40, Mn-3.5, Ni-1.0 and B-9.5 and a compound formula of $(\text{Cr}.53.\text{Fe}.42.\text{Mn}.04.\text{Ni}.01)_2\text{B}$.¹⁰ Reported results for Grade B ingot-metallurgy material identify the borides as a M_2B type where M is a metal²⁷ with a chromium level of approximately 50% and iron at about 40%. Analysis performed at Bohler Bleche identifies the borides as $(\text{Fe},\text{Cr},\text{Ni},\text{Mn},\text{Mo})_2(\text{B},\text{C})$.²⁸ The higher chromium level in the borides will deplete the base metal austenite next to the boride of this element.⁹

There was no evidence of a corrosion product detected on the surface of any of the Grade A borated stainless steel specimens in the testing program. As discussed in Section 3.2.5, the only damage was observed at the electrical connection point under the Teflon gasket. Representative images of the damage in this area are shown in Figures 25 and 26. The particles are the chromium-rich borides, and the corrosion mechanism appears to be localized corrosion around the borides, which allows them to fall free from the surface. The test solutions were filtered to gather a sample for XRD analysis, but the measurement results were inconclusive due to a very small sample size.

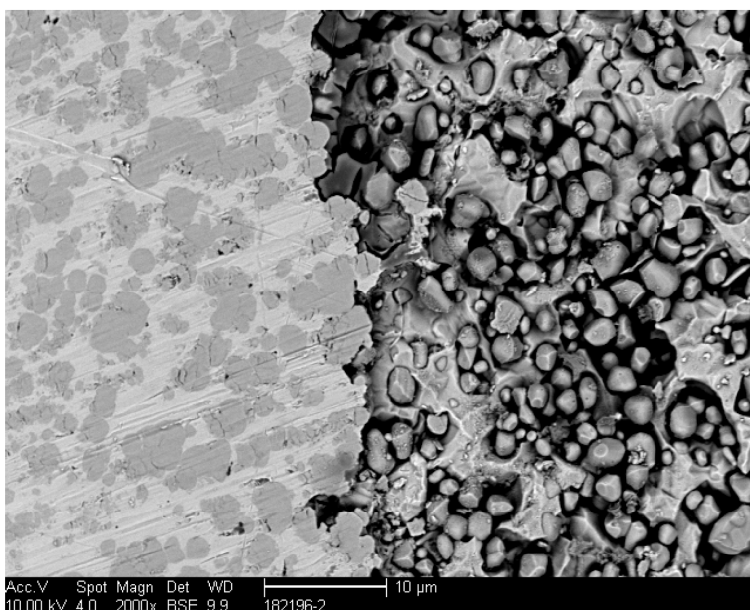


Figure 25. BSE image of localized corrosion near gasket in 304B6.

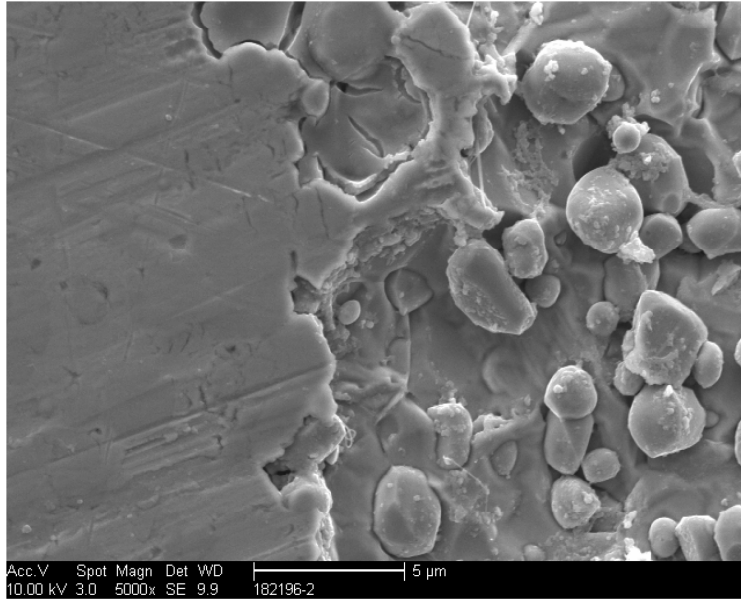


Figure 26. Secondary electron (SE) image of localized corrosion near gasket in 304B6.

4.1.2 Accelerated Corrosion Product Study

To increase the amount of corrosion product for XRD analysis, an accelerated corrosion test was performed using a 304B6 crevice-corrosion specimen polarized above the expected E_{corr} value (0.4 V versus SCE) at 90°C for 24 hours in solution B3. The 304B6 alloy was chosen as it shows a reduced resistance to localized corrosion compared to alloys 304B4 and 304B5 as reported in Section 3.2.6. This resulted in an excessive amount of crevice corrosion product that clouded the solution significantly (see Figure 27) and resulted in catastrophic attack to all surfaces of the specimen. The precipitate and corrosion product on the specimen was black and mostly lacked additional color. A total charge of 5616 C (355.4 C/cm^2) was passed during the test, with a maximum current of 5.29 A/cm^2 and a minimum of 2.25 A/cm^2 . Thus, localized corrosion was initiated instantly and remained active throughout the test. The specimen lost 1.83141 g during the test. Precipitate was collected during descaling, with sonication in 10% HNO_3 . After descaling cleanup, the specimen continued to produce small grey particles upon shaking. The particles from descaling were analyzed by XRD and matched with FeCr_2B . A similar match was made with settled precipitate collected at the bottom of the flask, which also indicated significant amounts of amorphous material.



Figure 27. Photographs of corrosion damage from 304B6 specimen in accelerated test: (A) corrosion flask, (B) specimen immediately after removal, and (C) and (D) two sides of specimen.

4.1.3 Neutronit Sample SSE 30 from the LTCTF

To further analyze the corrosion products that are evolved from the surface of a borated stainless steel undergoing localized corrosion, an examination was made on sample SSE-30, a Neutronit A978 sample (Heat E084295 in Table 1). This specimen was exposed at the water line to simulated cement modified water (SCMW) at 90°C for 2,134 days at the Long Term Corrosion Test Facility (LTCTF), formerly located at LLNL.^{13,29}

The specimens in the test program were affixed to an insulated and threaded rod through a central hole, as shown in Figure 28.²⁹ Note that part of the test specimen is cut away in the drawing for clarity. The specimens are held apart by Teflon spacers. The weight-loss specimen test assembly is fastened to a test rack, which is inserted into the large corrosion test vessels, as shown in Figure 29.